HHS Public Access

Author manuscript

*Science*. Author manuscript; available in PMC 2018 February 17.

Published in final edited form as:

*Science*. 2017 February 17; 355(6326): 739–743. doi:10.1126/science.aak9973.

# Treadmilling by FtsZ Filaments Drives Peptidoglycan Synthesis and Bacterial Cell Division

**Alexandre W. Bisson Filho**[*,1], **Yen-Pang Hsu**[*,3], **Georgia R. Squyres**[*,1], **Erkin Kuru**[*,3,7], **Fabai Wu**[5,8], **Calum Jukes**[6], **Yingjie Sun**[1], **Cees Dekker**[#,5], **Seamus Holden**[#,6], **Michael S. VanNieuwenhze**[#,2,3], **Yves V. Brun**[#,4], and **Ethan C. Garner**[#,1]

[1]Molecular and Cellular Biology (FAS) Center for Systems Biology, Harvard University, Cambridge, Massachusetts 02138 [2]Department of Chemistry, Indiana University, Bloomington, IN 47405 [3]Department of Molecular and Cellular Biochemistry, Indiana University, Bloomington, IN 47405 [4]Department of Biology, Indiana University, Bloomington, IN 47405 [5]Department of Bionanoscience, Kavli Institute of Nanoscience Delft, Delft University of Technology, The Netherlands [6]Centre for Bacterial Cell Biology, Institute for Cell and Molecular Biosciences, Newcastle University, Newcastle upon, Tyne NE2 4AX, UK

## Abstract

The mechanism by which bacteria divide is not well understood. Cell division is mediated by filaments of FtsZ and FtsA (FtsAZ) that recruit septal peptidoglycan synthesizing enzymes to the division site. To understand how these components coordinate to divide cells, we visualized their movements relative to the dynamics of cell wall synthesis during cytokinesis. We found that the division septum was built at discrete sites that moved around the division plane. FtsAZ filaments treadmilled circumferentially around the division ring, driving the motions of the peptidoglycan synthesizing enzymes. The FtsZ treadmilling rate controlled both the rate of peptidoglycan synthesis and cell division. Thus, FtsZ treadmilling guides the progressive insertion of new cell wall, building increasingly smaller concentric rings of peptidoglycan to divide the cell.

## Main Text

In most bacteria, cell division involves the inward synthesis of peptidoglycan (PG), creating a septum that cleaves the cell in two. The location of the septal PG synthases is regulated by

Correspondence should be addressed to egarner@g.harvard.edu, mvannieu@indiana.edu, ybrun@indiana.edu, seamus.holden@newcastle.ac.uk, and c.dekker@tudelft.nl.

[7]Current address: Department of Genetics, Harvard Medical School, Boston, MA 02115.

[8]Current address: Division of Geology and Planetary Sciences, California Institute of Technology, Pasadena, CA 91125.

[*]contributed equally

[#]co-corresponding authors.

Movies S1–S10 available at http://garnerlab.fas.harvard.edu/FtsZ/

Code available at https://bitbucket.org/garnerlab/bisson-2016

**Author Contributions**

This work represents the combined research directions of 3 groups (EG, YB/MV, SH/CD). FDAA labeling and 3D-SIM by YH and EK. Strains constructed by AB, GS, and CJ. Confocal and TIRF imaging by AB and GS. Microholes designed by SH and CD, fabricated by FW, and imaged by SH and CJ. Programming by GS, SH and YS. All authors designed experiments and wrote the paper.

filaments of the tubulin homolog FtsZ, which associate with the cytoplasmic side of the membrane via the actin-like FtsA and other factors. FtsZ forms membrane-associated filaments with FtsA (FtsAZ) (1, 2). Together, they form a dynamic structure, the Z ring, which encircles the cell at the future division site (3) and recruits PG synthases and other proteins involved in cytokinesis (4). Once the division machinery is mature, the Z ring constricts, while the associated synthases build the septum that partitions the cell in two.

We do not have a clear understanding of how the components of cell division interact in space and time to carry out cytokinesis, as we have been unable to observe the dynamics of each component relative to each other or to the structure they build: the organization and dynamics of FtsZ filaments within the Z ring remain ill-defined, it is not known how FtsAZ filaments control the activity of PG synthases, and the dynamics of septal PG synthesis have never been directly observed. To gain insight into how these components work together to divide bacteria, we visualized the dynamics of septal PG synthesis in relation to the movements of FtsAZ filaments and the septal PG synthase Pbp2B in the Gram-positive *Bacillus subtilis*.

To assess the dynamics of septal PG synthesis, we sequentially pulse-labeled growing cells with different colors of fluorescent D-amino acids (FDAAs) (Table S1), which are incorporated into PG (5) by the D,D-transpeptidation activity of Penicillin Binding Proteins (PBPs) (6). 3D-structured illumination microscopy (3D-SIM) showed that sequential three color FDAA pulse labeling resulted in bullseye patterns at the division plane (Fig. 1A), demonstrating the septum is progressively synthesized inward from the cell surface. Short, sequential pulses of two FDAA colors resulted in discrete spots or arcs distributed around the septum, with the colors more offset compared to cells pulsed simultaneously (Fig. 1B–C, S1A–B). Thus, PG synthesis occurs at discrete sites that move around the division plane.

We next observed how discrete sites of PG synthesis develop into a complete division septum by labeling cells with FDAAs using increasing pulse durations. Both the total amount of labeling and the area of labeled regions increased with pulse duration (Fig. 1D, left; Fig. S2A–C). Following short pulses, septa contained discrete spots or arcs (Fig. S1C). As pulse duration increased, these arcs elongated, gradually transitioning into complete rings at longer pulses (Fig. 1D, right). As expected, PG synthesis inhibitors reduced FDAA incorporation (Fig. S2D). To explore the location of the PG synthases relative to newly incorporated PG, we followed short FDAA pulses with Bocillin, which labels active PBPs (7) while inactivating them. The Bocillin signal was offset from the newly-synthesized PG (Fig. 1C, 1E), suggesting the PG synthases also move around the division plane.

We next examined the motions of the division-specific PG synthases and their associated cytoskeletal polymers. Total internal reflection fluorescence microscopy (TIRFM) of a functional mNeonGreen-FtsZ fusion expressed from the native locus (Fig. S3A–E, Tables S2–3) revealed directional movements within newly assembled Z rings (Fig. 2A, Movie S1). Furthermore, in almost every cell, we observed small mNeonGreen-FtsZ filaments outside the Z ring moving directionally around the cell at the same rate as within Z rings, similar to oscillations previously observed in *E. coli* (8). A functional FtsA-mNeonGreen fusion showed motions identical to FtsZ (Fig. 2B, Movie S1), and two-color imaging confirmed

FtsA and FtsZ colocalized and moved together (Fig. 2C) (9). Overexpression of a second *ftsAZ* operon (FtsA, mNeonGreen-FtsZ) resulted in many more directionally moving filaments outside the Z ring without affecting fitness (Fig. 2D, S3F). To resolve FtsZ motion in dense, actively constricting Z rings, we vertically immobilized bacteria in agarose microholes, orienting the division plane parallel to the objective (Fig. S4). This revealed multiple FtsZ filaments moving in both directions around the constriction site over a wide range of ring diameters (600–1000 nm) (Fig. 2E, S4E, Movie S2). The movement of multiple FtsZ filaments around Z ring may explain the heterogeneous structures and complex “patch” dynamics observed via super resolution microcopy (10–12), as well as the fast turnover of FtsZ subunits (13).

We next asked if the division-associated transpeptidase Pbp2B moves with FtsAZ. At native expression levels, mNeonGreen-Pbp2B moved directionally along the Z ring; this became more apparent with reduced expression (Fig. S5A–B). To observe the motions of single Pbp2B molecules, we labeled HaloTag-Pbp2B expressed from the native locus with low concentrations of HaloLigand-JF549 (14). TIRFM revealed two types of Pbp2B motion: 1) directional motion around the cell width, always localized to Z rings, and 2) diffusion on the membrane, not localized to Z rings (Fig. 2F, S5C–E, Movie S3). We did not observe diffusive Pbp2B motion along Z rings at any acquisition rate. In some cases, we observed multiple Pbp2B molecules moving directionally within the same ring, sometimes in opposite directions indicating that the Z ring contains multiple, independent synthetic sites. FtsZ, FtsA, and Pbp2B all moved at similar velocities (Fig. 2G, S5D–E), suggesting that their motions are associated.

We investigated the mechanism driving FtsAZ/Pbp2B motion, first testing if, similar to MreB (15), Pbp2B inactivation would halt FtsAZ motion. However, FtsAZ motion was unaffected by multiple PG synthesis inhibitors (Fig. 3A, 3H, Movie S4) or depletion of Pbp2B (Fig. 3B, 3H, Movie S5). We next tested if directional FtsAZ motion arose from filament treadmilling, as observed in vitro (16). Consistent with treadmilling, sparse labeling of FtsZ or FtsA in cells demonstrated that single molecules of both proteins were immobile within moving filaments (17) (Fig. 3C, S5F–J Movie S6). Because treadmilling requires nucleotide hydrolysis, we assayed FtsA motion as we modulated the GTPase activity of FtsZ. Exogenous expression of FtsZ(D213A), a mutant shown to have greatly reduced GTPase activity in *E. coli* (18), gradually reduced FtsAZ velocity, stopping motion at high inductions (Fig. 3D, 3G, Movie S7A). Likewise, addition of PC190723, an inhibitor of FtsZ GTP hydrolysis (19) halted FtsZ movement (Fig. 3E, Movie S8A). Conversely, addition of MciZ, a Z ring antagonist that, at low levels, increases FtsZ GTPase activity (20), increased FtsZ velocity (Fig. 3F, 3H, Movie S7B). We next tested whether FtsZ treadmilling dynamics affected Pbp2B movement. PC190723 or overexpression of FtsZ(D213A) caused Pbp2B molecules to become immobile while remaining FtsZ colocalized (Fig. 3D–E, Movie S8B). Pbp2B velocity scaled with FtsZ treadmilling velocity under various perturbations (Fig. S5K). Thus, FtsZ treadmilling is required for the directional motions of both FtsAZ filaments and septal PG synthases.

Given the mobile nature of septal PG synthesis, we reasoned that the directional movements of FtsAZ/Pbp2B around the division plane could be coupled to septal PG synthesis. To test

this, we labeled cells with FDAAs as we altered FtsZ dynamics. Overexpression of FtsZ(D213A) created long, slowly-growing FtsA-mNeonGreen spirals which incorporated FDAA along their entire length (Fig. 4A, Movie S9). Likewise, long PC190723 treatments resulted in fragmented patches of both FtsZ and FDAA incorporation (Fig. S6A), indicating Pbp2B activity is constrained by FtsAZ location. However, these strong inhibitions of FtsZ dynamics required much longer pulses to achieve FDAA labeling, suggesting that FtsZ treadmilling limits PG synthesis. To test this, we altered FtsAZ velocity as we pulse-labeled cells with FDAAs. This revealed that both the total amount and total area of PG synthesis within the ring are modulated by FtsAZ velocity: conditions that slowed dynamics decreased both the total amount and area of FDAA labeling (Fig. 4B, S6B–C). Conversely, increasing FtsAZ velocity (with MciZ) increased both the total amount and area of labeling. Thus, in *B. subtilis*, both the amount and spatial distribution of septal PG synthesis are directly coupled to, and limited by, the rate of FtsZ filament treadmilling.

Because FtsAZ dynamics control the rate of septal synthesis, we asked whether the rate of cytokinesis depended on FtsAZ treadmilling. We modulated treadmilling velocity by 1) introducing mutations affecting GTP hydrolysis into FtsZ at the native locus, 2) titrating exogenous FtsZ(D213A), 3) expressing MciZ, and 4) other perturbations (Table S4). This revealed the cytokinesis rate scaled with FtsZ treadmilling: division was slower when velocity was decreased, and faster when velocity was increased (Fig. 4C, S7A–C, Movie S10). Even under the strongest perturbations, these decreased rates of cytokinesis did not alter the rate of cell elongation (Fig. S7D–F). Thus, *in B. subtilis,* FtsAZ treadmilling is both coupled to, and limiting for, septal PG synthesis and cell constriction.

Our results indicate that cell division occurs by the action of discrete enzyme-filament complexes that, driven by FtsZ treadmilling, move around the division plane, building new PG during their transit (Fig. 4D). FtsZ treadmilling creates long range order from the local activity of the PG synthases, linking circumferential enzyme motion to the insertion of cell wall. This tight coupling may yield uniform insertion of new material around the division plane, building the septum inward in progressively smaller concentric rings. Cell division slightly differs in *E. coli,* where FtsZ treadmilling also distributes PG synthesis around the ring, perhaps because the rate of PG synthesis is limiting relative to FtsZ treadmilling (10). This difference may arise from different levels of cell wall precursors between the two organisms, or that *E. coli* must also couple PG synthesis to outer membrane insertion.

The coupling between FtsZ treadmilling and PG synthesis can unify previously conflicting models of cell division. FtsZ filaments have been proposed to generate force to bend membranes (2, 22), and to scaffold PG synthesis (10, 23). If FtsZ filaments deform membranes, coupling their movement to PG synthesis would allow each deformation to be reinforced via synthesis of PG (24). Thus, multiple sites of local deformation and coupled reinforcing synthesis moving around the division site would iteratively build the invaginating septum.

## Materials and Methods

**Culture growth—**All *B. subtilis* strains were prepared for experimentation as described below, unless otherwise noted. Strains were streaked from −80°C freezer stocks onto LB agar plates, and grown overnight at 37°C. Single colonies were transferred to liquid cultures in CH medium or PHMM Media - used to grow cells that were not chained (equal parts of CH and $S7_{50}$, with final concentrations of 1 mM glutamate, 0.5% glucose and 100 mM $MgCl_2$). Cells were placed on a roller drum for agitation and grown at 37°C. After cultures reached $OD_{600}$ < 0.5, serial dilutions were grown for one more round until $OD_{600}$ ~ 0.5. Alternatively, cultures were grown overnight at 25°C and then these starter cultures were diluted into the same media and grown at 37°C. bGS28 and bGS31 were grown with 50–100 μM IPTG to induce Pbp2B expression.

**Western blots—**Wild type (PY79), mNeonGreen-FtsZ (bAB185), FtsA-mNeonGreen (bAB167) and mNeonGreen-Pbp2B (ME7) were grown in 3 mL LB at 37°C until they reached $OD_{600}$ ~ 0.5, then diluted 10-fold to $OD_{600}$ ~ 0.05 and grown again until $OD_{600}$ ~ 0.5. Cultures were centrifuged at 13,000 rpm for 2 minutes, washed once with lysis buffer (20 mM Tris, pH 7.5, 100 mM NaCl, 10 mM EDTA, 1 mM PMSF) and pellets stored at −80°C overnight. Pellets were resuspended in 50 μl of lysis buffer with 10 μg/ml DNAse I, 100 μg/ml RNAse A and 10 mg/ml of lysozyme and incubated at 37°C for 20 minutes. Small aliquots were used to determine total protein mass (Pierce BCA Protein Assay Kit). 10, 25 and 50 μg of the lysates were then separated by SDS PAGE in 10% Bis-Tris gels, and blotted to 0.2 μm nitrocellulose membranes (Bio-Rad). The One-Hour Western Chemiluminescence Detection System kit (GenScript) was used coupled with primary antibiodies against FtsZ (anti-rabbit), FtsA (anti-mice) and Pbp2B (anti-rabbit). Antibodies were a gift from Jeff Errington, Frederico Gueiros Filho and Richard Daniel, respectively. Images were taken by a CCD camera coupled to the Chemilmager 5500 System (Alpha Innotech).

**Fluorescent D-amino acids synthesis—**HADA (7-hydroxycoumarin-3-carboxylic acid-D-alanine), BADA (BODIPY FL-D-alanine) and TADA (TAMRA-D-alanine) were synthesized as reported previously (5, 25). 7-hydroxycoumarin-3-carboxylic acid (for HADA, 1.45 mmole) or BODIPY FL (for BADA, 1.45 mmole) was added to a 100 ml, flame-dried round flask containing 14.5 ml anhydrous DMF and a stir bar. After adding 1.45 mmole carbonyldiimidazole to the flask, the reaction was stirred at room temperature (RT) for 2 hours, following by directly adding 1.45 mmole $N^{\alpha}$-Boc-D-2,3-diaminopropionic acid. The reaction was stirred overnight under argon atmosphere. The solvent was removed *in vacuo* and the product was extracted with EtOAc and 0.33N $HCl/H_2O$, and treated with trifluoroacetic acid and dichloromethane in 1:1 ratio for 30 min with stirring at RT. The final product was purified via reverse-phase HPLC with 10–90% $MeCN/H_2O$ gradient. For TADA synthesis, $N^{\alpha}$-Boc-D-2,3-diaminopropionic acid (1.45 mmole), 5-(and 6-) carboxytetramethylrhodamine succinimidyl ester (1.45 mmole), and diisopropylethylamine (200 μl) were added in one portion to a 100 ml round flask containing 14.5 ml anhydrous DMF. The reaction was stirred under argon overnight at RT. The product was de-protected and purified as described above.

**Fluorescent D-amino acids labeling—**FDAA stock solutions were prepared in DMSO (Sigma-Aldrich ReagentPlus >99.5%) at a concentration of 100 mM and stored at −20°C before use. The labeling conditions, including incubation interval and color order, are indicated in each FDAA figure and summarized in Table S1.

**FDAA-I—**For the sequential labeling in Fig. 1A, exponential phase cells (PY79) at $OD_{600}$ ~ 0.5 were diluted with PHMM containing 1 mM HADA to $OD_{600}$ ~ 0.1, and then grown for 1 hour at 37°C. Cells were washed twice with fresh PHMM (37°C), and centrifuged between washes (6,000 g for 1 minute at room temperature). For the second labeling, the cell pellets were resuspended in pre-warmed PHMM containing 1 mM BADA for 5 minutes. After this, cells were washed twice, and labeled a third time by resuspending in pre-warmed PHMM containing 2 mM TADA for 30 seconds. Cells were then immediately treated with 70% ice-cold ethanol, and incubated on ice for 1 hour. Ethanol-fixed cells were collected via centrifugation (10,000 g for 5 minutes at 4°C), washed twice with 4°C 1 × Phosphate Buffered Saline (PBS, pH 7.4), resuspended in PBS, and stored on ice before imaging.

**FDAA-II—**For the short-pulse labeling in Fig. 1B, 1E and S1A, cells (PY79) were first labeled with HADA (0.5mM, 60–90 minutes) and washed as described in **FDAA-I**. Cells were then transferred to a syringe filter (Acrodisc, 0.2 μm HT Tuffryn, 25 mm), and pre-warmed, fresh PHMM media (10 ml) was added to wash out excess dye. The cells were then treated sequentially with PHMM-FDAA media (2 mM BADA or TADA in 1 ml media for 15 sec), PHMM media (for washing), and PHMM-FDAA/Bocillin media (2 mM FDAA or 50 μg/ml Bocillin in 1 ml media for 15 sec) to label the cells. After washing with 10 ml PBS, cells were collected by back-sucking fixation reagent through the filter into the syringe. For Fig. 1B and S1A, 70% ethanol was used for fixation as described in **FDAA-I**. For Fig. 1E, to preserve the Bocillin signal, cells were fixed in 4% para-formaldehyde for 30 minutes at room temperature. Cells were collected by centrifugation (10,000 g for 5 minutes at 4°C), washed, and stored in PBS on ice before imaging.

**FDAA-III—**For time-course labeling in Fig. 1D, cells (PY79) were first labeled with HADA (1 mM, 60 minutes) as described above. The collected cells were resuspended in pre-warmed PHMM containing TADA (2 mM in 0.3 ml) and incubated for 15–120 seconds in a 37°C water bath. The cells were then fixed with 70% ethanol as described above. Labeling in Fig. S1B–C was performed similarly, using the FDAAs in a different order (see Table S1).

**FDAA-IV—**For FDAA labeling with antibiotic treatments in Fig. S2D, cells (PY79) were first labeled with HADA (1 mM, 60 minutes) as described above. Cell pellets were then resuspended in pre-warmed PHMM containing antibiotics (4 μg/ml Vancomycin or 50 μg/ml Penicillin G) and incubated for 3 minutes in a 37°C water bath. Next, TADA stock solution was added directly to the cells to a final concentration of 2 mM. After a 2 minute incubation, cells were fixed with 70% ethanol and collected as described above.

**FDAA-V—**For FDAA labeling with Pbp2B depletions in Fig. S2D, exponential phase cells (bGS3) were diluted with PHMM containing 1 mM HADA to $OD_{600}$ ~ 0.1, and grown for 3 hours at 37°C without IPTG to deplete Pbp2B. Following two washing steps with fresh PHMM (37°C), cell pellets were resuspended in pre-warmed PHMM containing 2 mM

TADA and incubated for 2 minutes. The cells were fixed with 4% para-formaldehyde as described above.

**FDAA-VI—**For FDAA labeling with FtsZ(D213A) expression in Fig. 4A, exponential phase cells (bAB217) were grown in PHMM containing 100 μM IPTG for 60 min, treated with TADA (2mM, 3 min), washed twice with pre-warmed PHMM, and then labeled with HADA (2 mM, 3 min). The cells were washed and then fixed with 4% para-formaldehyde as described above. For Fig. 4B, exponential phase cells (bAB217) were diluted with PHMM containing 1 mM HADA to $OD_{600}$ ~ 0.1. After 30 minutes of growth at 37°C, IPTG was added to the culture to a final concentration of 20 μM, and incubated for another hour. Following two washing steps with fresh PHMM (37°C) containing IPTG, cells were resuspended in fresh PHMM containing 2 mM TADA and IPTG, then incubated for 1 minute. The cells were then fixed with 70% ethanol and washed.

**FDAA-VII—**For FDAA labeling with PC190723 treatment in Fig. 4B, exponential phase cells (PY79) were diluted with PHMM containing 1 mM HADA to $OD_{600}$ ~ 0.05. After a 90-minute growth at 37°C, PC190723 (10 mg/ml, DMSO stock) was added to the culture to a final concentration of 1 μg/ml, and incubated for another 10 min. Following two washing steps with fresh PHMM (37°C) containing PC190723, cells were resuspended in fresh PHMM containing 2 mM TADA and PC190723, then incubated for 1 minute. The cells were then fixed with 70% ethanol as described above. Labeling in Fig. S6A was performed similarly, using 10 μg/ml PC190723 and 2 min of TADA labeling.

**FDAA-VIII—**For FDAA labeling with MciZ expression in Fig. 4B, exponential phase cells (strain AH93) were diluted with PHMM containing 1 mM HADA to $OD_{600}$ ~ 0.05. After a 90-minute incubation at 37°C, 50 mM xylose was added to the culture, and the cells were incubated for 5 minutes. Following two washing steps with fresh PHMM (37°C) containing xylose, cells were resuspended in fresh PHMM containing 2 mM TADA and 50 mM xylose, then incubated for 30 seconds. The cells were fixed with 70% ethanol as described above.

**HaloTag labeling with Halo-TMR and JF- dyes—**For the Fig. 2D, full labeling of FtsA-HaloTag(SW) (see strain construction for details) was obtained by incubating strain bAB229 with 500 nM HaloTag-JF549 ligand for 15 min. For Fig. 2F and 3E, Pbp2B single molecules were obtained by incubating bGS31 (*HaloTag-pbp2B*) with 40–100 pM of HaloTag-JF549 ligand for 15 min; cells were washed once in fresh media to remove free dye before imaging. For Fig. 3C, FtsA single molecules were obtained by incubating bAB213 (*ftsA-HaloTag(SW)*) with 250 pM of HaloTag-JF646 ligand for 15 min. HaloTag ligands were a gift of Luke Lavis (14).

**Depletions in liquid culture—**For the Pbp2B depletions shown in Fig. 3B and Movie S5, bGS31 cells (*ftsZ::mNeonGreen-ftsZ*, *erm-Phyperspank-HaloTag-pbp2B*) were grown in liquid culture with 10 μM IPTG until $OD_{600}$ ~ 0.5, the inducer was washed out, and then cells were shifted to media lacking IPTG. Before imaging mNeonGreen-FtsZ, cells were observed under microscope every 30 minutes until no divisions were observed to ensure Pbp2B depletion.

**Expression of *ftsAZ* constructs—**For all experiments in which the expression of a second copy of tagged FtsA and/or FtsZ was required, fusions were made in a way to maintain the operon structure to avoid perturbations on the FtsA/FtsZ ratio (26, 27). As shown in Fig. S3F, increased levels of either FtsA or FtsZ can impair cell division, while high levels of FtsAZ did not present an observable phenotype.

**Perturbations in CellASIC microfluidic system—**To observe the effects of MciZ (Fig. 3F, Movie S7B) and PC190723 (Fig. 3E, Movie S8A) on FtsAZ motion, we used the microfluidic CellASIC system from EMD Millipore with B04A plates. Cells in optimal growth conditions (as described in the culture growth section) were loaded into the device and equilibrated for 1 hour in CH media at a flow of 3 PSI. Afterward, based on the observation that exogenous MciZ is capable of penetrating cells and inhibiting Z ring assembly (28), cells were flowed with 1 μM of synthetic MciZ peptide or 10 μM of PC190723 at 5 PSI and imaged by TIRF microscopy. Pulses and washes were performed as needed and described in each figure legend. Synthetic MciZ peptide and PC190723 drug were purchased from PSL Peptide Specialty Laboratories GmbH and EMD Millipore, respectively.

**Antibiotic treatments—**For the effect of different antibiotics on FtsAZ motion (Fig. 3A and Movie S4), cells were grown in liquid as described above and placed under agarose pads (500 μl of media with 2% agarose). After FtsAZ motion was confirmed by TIRF microscopy, 3 μl of the antibiotic was added on top of the pad, followed by 5 minutes of incubation. Time lapses were then acquired from different fields of view. Antibiotic concentrations were as follows: 10 mg/μl Ampicillin (blocks transpeptidation); 10 mg/μl Penicillin G (blocks transpeptidation); 50 mg/μl Vancomycin (blocks transpeptidation and transglycosylation); 100 mg/μl Fosfomycin (blocks PG precursor synthesis); 100 mg/μl Cephalexin (blocks transpeptidation). To confirm the effect of each specific treatment, we conducted separate experiments where we incubated liquid cultures with each antibiotic (at a final concentration of 10 μg/μl) for 5 minutes, followed by imaging.

**Correlation between FtsAZ motion and cytokinesis rates—**For the effects of different genetic backgrounds and overexpression of a number of components on FtsAZ motion and cytokinesis rates (shown in Fig. 4C, Table S4, Movie S10), cells were grown in liquid as described above and placed under agarose pads. Where inducible promoters were used, the appropriate IPTG concentration (0, 1, 5, 7.5, 10 and 100 μM) was mixed into to the pad. The exception to this protocol was the experiments with MciZ-expressing cells. Because very low concentrations of MciZ can quickly block cell division (20, 29), MciZ was only induced after cells were under the agarose pad, by addition of 5 μl of a 3M xylose solution on top of the 500 μL pad (as with the antibiotic perturbations described above). Each condition was imaged on a spinning disk confocal (for Pbp2B ring constriction) and on a TIRF microscope (for FtsAZ filament dynamics). The strains, conditions, and measurements for each experiment are shown in Table S4. mNeonGreen-Pbp2B was used as a reporter of cytokinesis, and the constriction times were measured by manual kymographs. These measurements were then validated by automated analysis. **Manual tracking:** For each condition, 100 random rings were cropped, and kymographs were drawn along the ring

axis using Fiji. From these kymographs we determined when ring constriction initiated by using the time point where the slope of the edge of the signal switched from being vertical to angled (top dotted line). The disappearance of Pbp2B was used to indicate the end constriction period (assayed by the last bright pixel in the kymograph). The difference in these two time points was taken as the constriction interval for each ring. **Automated analysis**: To independently validate these manual measurements, we applied an automated analysis of the cytokinesis time. We exploited the fact that mNeonGreen-Pbp2B rings get brighter up until they begin constriction to set a threshold for each image based on the average of intensity of 100 constricting rings. We then applied this threshold to entire fields of cells. We then tracked these thresholded rings with the TrackMate plugin to determine each ring's lifetime (30). We set a lifetime cutoff between 5–30 minutes, to exclude rings that that were already at late stages of constriction, or anomalous constrictions.

**Microholes nanofabrication—**Microholes are patterned through electron-beam lithography as described previously (31) and etched through a reactive-ion etching (32). Briefly, a silicon wafer was spin-coated with resist NEB-22 (Sumitomo Chemical). Predesigned features were patterned through Leica EBPG 5000+ with a beam step size of 20 nm. The exposed resist was removed by solvent Microposit MF-322 solution and the exposed wafer surface was etched using an AMS Bosch Etcher. The remaining resist was removed using oxygen plasma.

**Culture growth for vertical microhole immobilization—***B. subtilis* strains to be imaged by vertical microhole immobilization were streaked from −80°C freezer stocks onto LB agar plates, grown at 30°C in Time Lapse Medium (TLM) (33) overnight, re-diluted in pre-warmed Chemically Defined Medium (CDM) (33) and grown at 30°C to $OD_{600}$ ~ 0.4 before being immobilized in agarose microholes (see below).

**Imaging – slide preparation—**Coverslips were sonicated in 2% Hellmanex (Hellma GmbH&Co, Milllheim, FRG) for 30 minutes, followed by multiple washes with deionized water, then sonicated with 1 M KOH for 30 minutes, followed by multiple washes with water. Coverslips were washed twice with 100% ethanol, and then sonicated for 30 minutes in 100% ethanol, followed by one more wash in 100% ethanol. They were stored in ethanol and dried before use.

**Imaging – Pbp2B and FtsZ ring constriction rates—**Images were collected on a Nikon TI spinning disk confocal microscope with Yokogawa CSU-10 spinning disk and a Hamamatsu ImagEM (EM-CCD) camera (effective pixel size 110 nm), and Nikon 100X NA 1.45 TIRF objective. Illumination was accomplished using fiber coupled Spectral lasers, using a 488 laser for imaging of mNeonGreen, and a 494 nm laser for imaging of FM5-95. For the experiments following ring constriction, time lapses were acquired with 1 minute intervals for 2 hours with exposure times of 50–150 milliseconds.

**Imaging – FtsAZ and Pbp2B dynamics by TIRFm—**Images were collected on a Nikon TI microscope equipped with a 6.5 μm pixel CMOS camera and an EMCCD camera, together with a Nikon 60X NA 1.40 and a Nikon 100X NA 1.45 objective set. Exposure times varied between 0.1 and 3 seconds, as indicated. Illumination was accomplished using a

fiber coupled Agilent launch with for 405 nm, 488 nm (imaging of mNeonGreen and msfGFP fluorescent proteins), 561 nm (imaging of JF549 dye) and 647 nm (imaging of JF646 dye).

**Imaging – 3D-SIM of FDAA labeling—**3D-SIM images were collected on DeltaVision OMX system (Applied Precision Inc, Issaquah, USA) equipped with 1.4 NA Olympus 100X oil objective, laser source (405, 488, 561 and 642 nm) and four photometrics Cascade II EM-CCD cameras. 24X50 mm coverslips (# 1.5) were used as imaging support for the inverted system. Cell samples were loaded on the coverslips, followed by laying an 8X8 mm wide, 2 mm thick PBS-agar pad on top of the cells. The coverslip-pad combination was placed onto the OMX microscope in a sample stage plate with the pad facing upwards. 3D-SIM imaging was controlled with the DV-OMX software. FDAA signal was captured by using: 1) for HADA, 405 nm laser with 419–465 nm emission filter; 2) for BADA, 488 nm laser with 500–550 nm filter; and 3) for TADA, 561 nm laser with 609–654 nm filter. The z-axis scanning depth ranged from 2.4 to 3 μm. The immersion oil was optimized for each experiment with a range from 1.514 to 1.518.

**Imaging – agarose microhole sample preparation—**Agarose microholes were created by pouring molten 6% agarose onto a silicon micropillar array (Fig. S4). Patterned agarose was transferred into a Geneframe (Thermo Scientific AB-0577) mounted on a glass slide. The regions either side of the microholes were cut away, leaving a thin strip of agarose in the center of the Geneframe, to ensure sufficient oxygen. Cells at $OD_{600}$~0.4 were concentrated 100× by centrifugation. 4 μL of sample was then loaded onto the agarose pad and a cover slip was placed on top.

**Imaging – FtsZ dynamics in agarose microholes—**FtsZ dynamics were imaged by near-TIRF illumination on a Nikon N-STORM microscope equipped with an NA 1.49 Nikon 100× TIRF objective, laser source (488 nm), additional 2.5× magnification optics and a 16 μm pixel Andor iXon DU897 EMCCD, giving a final pixel size at the image plane of 64 nm. Exposure times were 1 s and images were taken at 1 s intervals. The temperature at the sample was 30.0°C.

**Image processing—**All image processing unless otherwise specified was performed in Fiji (34). Images used for particle tracking were unaltered, except for trimming two pixels from the edges of some videos to remove edge artifacts detected by the tracking software. Images were cropped, contrast adjusted, rotated and scaled (no interpolation) for figures. SIM images were reconstructed using softWoRx and the quality was confirmed by SIMcheck (35). 3D projections were obtained with the Volume Viewer function of softWoRx with 25 stacks. The image of the $13^{th}$ stack (90°-rotated) was used for data analysis.

**Data analysis – kymographs—**Kymographs were generated by the Fiji *kymograph* plugin with a line width of 3 (for FtsA and FtsZ) or 5 (for Pbp2B). For kymograph-based velocity measurements, velocities were quantitated by measuring the length of fluorescent trajectories in pixels and converting to nm and sec, respectively. For constriction times, kymographs of each condition were plotted and the intervals converted from the length of

line segments in pixels: see “Correlation between FtsAZ motion and cytokinesis rates” above for details.

**Data analysis – particle tracking—**For particle tracking, tracks were generated using the TrackMate plugin in Fiji (30). Particles were detected with the Laplacian of Gaussians (LoG) detector, with a 400 nm blob diameter. Tracks were generated using the Linear motion LAP Tracker, with a 100 nm search radius and no frame gaps allowed. Tracks were then exported into MATLAB for further processing. For the characterization of FtsZ and A single molecules, we included all tracks containing 5 or more frames, since frames 4 and under cannot be fit by the velocity calculating algorithm; no additional filtering was done. For the characterization of FtsZ, FtsA and Pbp2B velocity, we applied additional filters to select for tracks with quantifiable directional motion. Using a custom script, tracks were filtered to select for directionally-moving tracks and exclude background, erroneous assignments, and, in the case of Pbp2B, rapidly diffusing molecules outside of the Z ring. Tracks shorter than 10 seconds or longer than 25 seconds were excluded, as were tracks whose start to endpoint displacement was less than 50 nm. For each track, the velocity, the diffusion coefficient, and the scaling exponent α were calculated as described previously (15). Briefly, mean squared displacement vs time delay (MSD vs $t$) was calculated for each track. Linear fits were made to log(MSD($t$)) vs log($t$); α is the slope of this fit. To ensure the quality of the tracks, only tracks with $r^2 > 0.95$ for this linear fit were included in the data set. Velocity and diffusion coefficient were then calculated by fitting $MSD(t) = 4D(t) + (Vt)^2$ using nonlinear least-squares fitting (15).

**Data analysis – photobleaching traces—**Images for photobleaching analysis were collected with 200 ms exposures, acquiring continuously (5 frames/second) to ensure sufficient time resolution. Representative particles were chosen manually. Using Fiji, intensity traces were generated from a 5×5 pixel region that was centered on the particle. To reduce noise, intensity traces were then filtered using a median intensity filter with a 4 second time window. The filtered trajectories were normalized to their minimum and maximum values: this was necessary because, particularly in TIRF, illumination intensity is non-uniform across the field of view. For plotting, intensity traces were aligned such that time t=0 corresponds to the frame in which the particle appears.

**Data analysis – vertical microhole imaging—**Images were corrected for translational drift using the Fiji *StackReg* plugin. Kymographs were automatically calculated along the circumference of individual Z rings using a custom MATLAB script. The best fitting circle for each Z ring was identified by least squares fitting, and the intensity around the circumference of the ring calculated with sub-pixel precision by bicubic interpolation. FtsZ velocities were calculated as per the kymographs above. Mean filament speed in Fig. S4E measured by Gaussian fitting.

**Data analysis – plots—**Plots were generated using Prism and MATLAB. Violin plots were generated in MATLAB using the violin.m function (36). Horizontal error bars were added to Fig. 4C using the ploterr.m function (37). In plots, ns and * is used to indicate the

result of an unpaired two-sample t-test: ns $p \geq 0.05$, *$p < 0.05$, **$p < 0.01$, ***$p < 0.001$, ****$p < 0.0001$.

**Data analysis – 3D-SIM—**To confirm that 3D-SIM images could be used for intensity quantitation, we demonstrated that intensity of Tetraspeck beads scaled linearly with exposure time after reconstruction (Fig. S2A). For quantitative analyses, septal PG images were collected by cropping the division site of the cells (~1.5 × 0.5 μm) using softWoRx software (Applied Precision, Issaquah, WA). Long-pulse labeling of FDAA (usually HADA) was used to identify the division sites and cell division state. Only the cells having a clear division site but not yet a complete septum were collected and analyzed. To quantify total intensity, we summed the intensity of 3D projections of Z rings. To quantify area labeled, we counted the number of pixels in the image that were above a set intensity threshold. Because the choice of threshold was arbitrary, where this metric was used, we demonstrated that the observed trends were independent of threshold choice (Fig. S2B). For total area labeled, we summed all the labeled pixels in the image; this represents total amount of FDAA labeling. For average feature area, we counted the number of pixels in each discrete labeled region of FDAA; this indicates the amount of FDAA labeling per spot. For the time course data in Fig. 1D and S2B–C, images from the longer labeling times (60, 90, and 120 seconds) were acquired with half the exposure time of the shorter labeling times to avoid saturating intensities. To compare these time points, we corrected the intensity for the later time points by multiplying their values by 2; we confirm that intensity scales linearly with exposure time in Fig. S2A. Violin plots were generated in MATLAB using the violin.m function (36). To compute the correlation between images, we first background subtracted each image in Fiji (rolling ball radius = 10). The correlation coefficient was then computed in MATLAB.

**Data analysis – blinded manual classification—**All images to be classified were combined into a single data set. First, the user was given instructions on how to use the software and shown sample images that typified each category. Next, the user classified 20 images in a practice round, using a custom MATLAB GUI; these responses were not recorded. The user was then asked to sort each image in the data set into one of the categories, with the option to skip images they felt could not be classified. All images in the combined data set were shuffled and presented to the user in a random order, with no information about which experimental condition they came from.

**Data analysis – correlation between filament speed and cytokinesis—**FtsZ filament average velocities and constriction times were obtained from kymographs as described above (see “Correlation between FtsAZ motion and cytokinesis rates” and “Data analysis – kymographs”). Filament velocities versus constriction times were plotted using MATLAB. An exponential fit to the data was generated in MATLAB.

**Data analysis – single cell growth rates—**Wild type (PY79), FtsZ(D213A) (10 μM IPTG, strain bAB273) and FtsZ(T111A) (strain bAB270) cells were grown in LB at 37°C, placed onto LB+2% agarose pads and imaged with phase contrast for 90 minutes at 2 minute intervals. Individual cell growth was analyzed by a custom MATLAB program. First, the area of the cells was measured based on the segmentation of phase contrast images. Cells

were then tracked over time. The growth rate of each cell is calculated by the slope of the linear fit of the natural logarithm of total areas. For each linear fit of the total area of cells, the R squared threshold is set to 0.95.

## Sequences of Fluorescent Proteins, Tags and Linkers

### msfGFP—

ATGCGAAAAGGGGAAGAATTGTTTACAGGCGTAGTACCGATATTAGTTGAGCTGG
A
TGGAGATGTTAACGGACACAAGTTTTCCGTACGCGGAGAGGGAGAAGGCGATGC
CA
CCAATGGCAAACTCACCCTTAAATTTATTTGTACGACAGGCAAGCTACCAGTGCCG
T
GGCCTACATTGGTCACTACACTCACGTATGGTGTGCAATGCTTTGCAAGATATCCC
G
ACCACATGAAGCAACATGACTTTTTCAAATCAGCCATGCCTGAAGGATATGTCCAA
G
AAAGGACTATTAGCTTTAAGGACGACGGCACCTACAAAACACGCGCTGAAGTCAA
A
TTCGAAGGTGATACGTTAGTTAATCGTATCGAACTGAAAGGTATAGACTTTAAAGA
A
GATGGAAATATCCTGGGGCATAAGTTGGAGTACAATTTCAACAGCCATAACGTATA
CATCACAGCTGACAAGCAGAAAAATGGCATTAAAGCAAATTTCAAAATCAGACAT
A
ACGTTGAAGATGGGTCAGTTCAGCTTGCGGATCATTATCAACAGAACACACCGAT
TG
GCGATGGTCCGGTGTTACTACCTGATAACCATTATCTGTCGACTCAGAGTAAACTG
T
CTAAAGATCCAAATGAAAAACGGGACCACATGGTCCTTTTAGAGTTTGTGACGGC
A GCTGGGATTACGCATGGAATGGATGAACTTTACAAATAA

### mNeonGreen—

ATGGTTTCGAAAGGAGAGGAGGATAATATGGCTAGCCTCCCAGCGACCCACGAAC
T
GCATATTTTTGGCAGCATTAATGGCGTTGACTTTGATATGGTGGGGCAGGGAACAG
G
GAACCCTAACGATGGCTATGAGGAGCTCAATCTCAAGAGTACAAAAGGAGATTTG
C
AATTTTCACCTTGGATCCTGGTTCCGCATATTGGCTACGGCTTTCATCAATACTTGC
C
TTATCCGGACGGCATGTCCCCGTTCCAAGCTGCGATGGTGGATGGTTCTGGGTACC
A
GGTGCACCGTACTATGCAGTTTGAGGACGGTGCCTCACTGACGGTCAACTATAGAT
A
TACTTATGAAGGCTCACACATTAAGGGTGAGGCCCAAGTTAAAGGAACAGGGTTT
C

CTGCGGATGGACCGGTAATGACAAACAGTTTAACCGCTGCGGACTGGTGTCGCTC
G
AAAAAAACATACCCAAACGATAAAACGATCATCTCGACCTTCAAATGGAGCTATA
C
TACGGGCAACGGCAAACGCTATCGTTCCACAGCACGCACGACTTATACGTTTGCTA
A
ACCGATGGCCGCAAACTACCTCAAAAATCAACCTATGTACGTGTTCAGAAAAACC
G
AGTTAAAACATTCAAAAACGGAACTTAATTTTAAAGAGTGGCAAAAGGCGTTTAC
A GACGTGATGGGTATGGATGAACTCTATAAGTGA

**HaloTag—**

ATGGCAGAAATCGGTACTGGCTTTCCATTCGACCCGCATTATGTGGAAGTCCTGGG
C
GAGAGAATGCATTACGTTGACGTGGGTCCGAGAGATGGAACTCCGGTCCTTTTTC
TG
CACGGGAATCCTACAAGCTCTTATGTTTGGCGCAATATCATCCCTCATGTAGCTCC
G
ACGCATCGCTGTATTGCGCCGGACCTGATTGGTATGGGAAAATCTGATAAACCAG
AC
CTGGGTTACTTTTTCGATGATCATGTGCGTTTCATGGATGCCTTCATTGAGGCATTA
G
GGCTTGAAGAAGTCGTCTTGGTGATTCATGATTGGGGCTCAGCTCTGGGATTTCA
CT
GGGCTAAAAGAAATCCTGAACGCGTAAAAGGCATCGCGTTTATGGAGTTCATTCG
TC
CAATTCCGACTTGGGATGAATGGCCTGAGTTCGCGAGAGAAACATTTCAAGCATT
TC
GCACGACCGATGTAGGCCGGAAGTTAATCATCGATCAGAATGTCTTTATCGAAGGG
ACATTGCCGATGGGAGTCGTTCGTCCGTTAACAGAAGTCGAAATGGATCACTATAG
A
GAACCTTTTCTTAATCCTGTGGACAGAGAGCCGCTGTGGCGGTTTCCGAACGAAC
TG
CCGATTGCAGGCGAGCCTGCTAACATTGTAGCGCTGGTTGAAGAGTATATGGATTG
G
CTTCATCAGTCTCCAGTTCCGAAGTTATTGTTTTGGGGTACGCCTGGCGTGCTTAT
TC
CACCGGCCGAAGCGGCACGTTTGGCAAAAAGCCTGCCAAATTGCAAAGCCGTTG
AC
ATTGGCCCTGGACTTAACTTGCTTCAAGAGGATAACCCGGACTTAATCGGGAGCG
AA ATTGCCCGGTGGCTTTCTACCTTAGAAATCAGCGGCTAG

**15aa Linker A—**

CTCGAGGGATCTGGCCAGGGACCGGGCTCAGGCCAAGGAAGCGGC

**15aa Linker B—**

CTTGAGGGTAGCGGACAAGGTCCTGGATCTGGTCAAGGCAGTGGG

## Strain Construction

**ME7** [*pbp2B::mNeonGreen-15aa-pbp2B*] was created by transforming PY79 with a Gibson assembly consisting of 4 fragments: 1) PCR with primers oME32 and oME22 and PY79 genomic DNA template (containing the region upstream of the *pbp2B* gene); 2) PCR with primers oZB46 and oZB47 and bMK93 genomic DNA template (containing the construct of first 30 bp *mNeonGreen-cat cassette-*$P_{xylA}$ *promoter-mazF gene-*$P_{veg}$ *promoter*); 3) PCR with primers oZB33 and oZB34 and the synthetic *mNeonGreen* gene as template (ordered from IDT, see fluorophore sequences section); 4) PCR with primers oME20 and oME21 and PY79 genomic DNA template (containing the *pbp2B* gene). Transformations were plated on LB-Cm plates with 2% glucose and incubated at 37°C. Transformants were grown in LB with 2% glucose until $OD_{600}$ ~ 0.5, plated on LB plates with 2% xylose, and incubated at 37°C. Colonies were then patched onto LB, LB-Cm and LB-Xylose plates and candidates that were sensitive to Cm but resistant to xylose were stocked and confirmed by PCR and sequencing.

**bGS3** [*pbp2B::erm-*$P_{hyperspank}$*-mNeonGreen-15aa-pbp2B*] was created by transforming PY79 with a Gibson assembly consisting of 3 fragments: 1) PCR with primers oAB81 and oAB82 and PY79 genomic DNA template (containing the region upstream of the *pbp2B* gene); 2) PCR with primers oJM29 and oMD232 and bMD352 genomic DNA template (containing the construct *erm-*$P_{hyperskpank}$); 3) PCR with primers oAB137 and oAB87 and ME7 genomic DNA template (containing the *mNeonGreen-15aa-pbp2B* fusion). Transformations were plated on LB-MLS plates with 100 μM IPTG and colonies were patched onto LB and LB+IPTG plates. Candidates that presented resistance to MLS and IPTG dependence were confirmed by PCR and sequencing.

**bGS28** [*pbp2B::erm-Phyperspank-HaloTag-15aa-pbp2B*] was created by transforming PY79 with a Gibson assembly consisting of 4 fragments: 1) PCR with primers oAB81 and oAB82 and PY79 genomic DNA template (containing the region upstream of the *pbp2B* gene); 2) PCR with primers oJM29 and oMD232 and bMD352 genomic DNA template (containing the construct *erm-*$P_{hyperskpank}$); 3) PCR with primers oGS7 and oAB14 and the synthetic *HaloTag* gene as template (ordered from DNA 2.0, see fluorophore sequences section); 4) PCR with primers oME20 and oAB87 and PY79 genomic DNA template (containing the *pbp2B* gene). Transformations were plated on LB-MLS plates with 100 μM IPTG and colonies were patched onto LB and LB+IPTG plates. Candidates that presented resistance to MLS and IPTG dependence were confirmed by PCR and sequencing.

**bGS60** [*pbp2B::erm-Phyperspank-HaloTag-15aa-pbp2B, ftsZΩftsZ(T111A) (tet)*] was created by transforming bGS28 with genomic DNA from AB62 (a gift from Frederico Gueiros Filho).

**bGS90** [*pbp2B::erm-Phyperspank-HaloTag-15aa-pbp2B, amyE::erm-*$P_{hyperspank}$*-ftsAZ(D213A)*] was created by transforming bGS28 with genomic DNA from bAB215.

**bGS31** [*pbp2B::erm-Phyperspank-HaloTag-15aa-pbp2B, ftsZ::mNeonGreen-15aa-ftsZ]* was created by transforming bAB185 with genomic DNA from bGS28.

**bAB94** [*amyE::erm-*$P_{hyperspank}$*-ftsA*] was created by transforming PY79 with a Gibson assembly consisting of 3 fragments: 1) PCR with primers oMD191 and oMD232 and bMD352 genomic DNA template (containing the region upstream of the *amyE* gene, the *erm* cassette and the $P_{hyperspank}$ promoter); 2) PCR with primers oAB78 and oAB93 and PY79 genomic DNA template (containing the *ftsA* gene); 3) PCR with primers oMD196 and oMD197 and PY79 genomic DNA template (containing the region downstream of *amyE*).

**bAB96** [*amyE::erm-*$P_{hyperspank}$*-ftsZ*] was created by transforming PY79 with a Gibson assembly consisting of 3 fragments: 1) PCR with primers oMD191 and oMD232 and bMD352 genomic DNA template (containing the region upstream of the *amyE* gene, the *erm* cassette and the $P_{hyperspank}$ promoter); 2) PCR with primers oAB95 and oAB94 and PY79 genomic DNA template (containing the *ftsA* gene); 3) PCR with primers oMD196 and oMD197 and PY79 genomic DNA template (containing the region downstream of *amyE*).

**bAB98** [*amyE::erm-*$P_{hyperspank}$*-ftsAZ*] was created by transforming PY79 with a Gibson assembly consisting of 3 fragments: 1) PCR with primers oMD191 and oMD232 and bMD352 genomic DNA template (containing the region upstream of the *amyE* gene, the *erm* cassette and the $P_{hyperspank}$ promoter); 2) PCR with primers oAB78 and oAB94 and PY79 genomic DNA template (containing the *ftsAZ* operon); 3) PCR with primers oMD196 and oMD197 and PY79 genomic DNA template (containing the region downstream of *amyE*).

**bAB146** [*amyE::erm-*$P_{hyperspank}$*-mNeonGreen-15aa-pbp2B*] was created by transforming PY79 with a Gibson assembly consisting of 3 fragments: 1) PCR with primers oMD191 and oMD232 and bMD352 genomic DNA template (containing the upstream region to *amyE* gene, the *erm* cassette and the $P_{hyperspank}$ promoter); 2) PCR with primers oAB137 and oAB134 and ME7 genomic DNA template (containing the mNeonGreen-15aa-pbp2B construct); 3) PCR with primers oMD196 and oMD197 and PY79 genomic DNA template (containing the region downstream to *amyE*).

**bAB167** [*ftsA::ftsA-mNeonGreen(SW)*] was created by inserting mNeonGreen between helices 6 and 7 of FtsA, the equivalent of a sandwich fusion (SW) that proved to be functional for MreB-mCherry (38). PY79 cells were transformed with a Gibson assembly consisting of 7 fragments: 1) PCR with primers oAB74 and oAB75 and template PY79 genomic DNA (containing the region upstream of the *ftsAZ* promoters); 2) PCR with primers oJM28 and oJM29 and template pWX467a (containing the *erm* cassette); 3) PCR with primers oAB76 and oAB33 and template PY79 genomic DNA (containing the first 801 bp of the *ftsA* gene); 4) PCR with primers oAB135 and oAB136 and the synthetic *mNeonGreen* gene as template (ordered from IDT, see fluorophore sequences section); 5) PCR with primers oAB48 and oAB28 and template PY79 genomic DNA (containing the last 522 bp of the *ftsA* gene and the *ftsZ* region); 6) PCR with primers oJM28 and oJM29 and template pWX465a (containing the *cat* cassette); 7) PCR with primers oAB29 and oAB30 and template PY79 genomic DNA (containing the region downstream of *ftsAZ* terminators). After proper integration was confirmed by PCR and sequencing, the resistance cassettes

were looped-out using pDR244 (containing Cre recombinase, a gift from David Rudner), and incubating transformed cells overnight at 30°C. Colonies were streaked onto LB, LB-MLS, LB-Cm and LB-Spec plates and incubated overnight at 45°C. After confirming that only LB plates presented colonies, the loop-outs were confirmed by PCR and sequencing.

**bAB185** [*ftsZ::mNeonGreen-15aa-ftsZ*] was created by transforming PY79 with a Gibson assembly consisting of 7 fragments: 1) PCR with primers oAB74 and oAB75 and template PY79 genomic DNA (containing the region upstream of the *ftsAZ* promoters); 2) PCR with primers oJM28 and oJM29 and template pWX467a (containing the *erm* cassette); 3) PCR with primers oAB76 and oAB139 and template PY79 genomic DNA (containing the region upstream of the *ftsZ* gene); 4) PCR with primers oZB33 and oZB34 and the synthetic *mNeonGreen* gene as template (ordered from IDT, see fluorophore sequences section); 5) PCR with primers oAB140 and oAB28 and template PY79 genomic DNA (containing the *ftsZ* gene region); 6) PCR with primers oJM28 and oJM29 and template pWX465a (containing the *cat* cassette); 7) PCR with primers oAB29 and oAB30 and template PY79 genomic DNA (containing the region downstream of the *ftsAZ* terminators). After proper integration was confirmed by PCR and sequencing, the resistance cassettes were looped out by transforming the plasmid pDR244 (containing Cre recombinase and a temperature sensitive origin of replication, a gift from David Rudner), and incubating transformed cells overnight at 30°C. Colonies were streaked onto LB, LB-MLS, LB-Cm and LB-Spec plates and incubated overnight at 45°C to remove the plasmid. After confirming that only LB plates presented colonies, the loop-outs were confirmed by PCR and sequencing.

**bAB199** [*ftsZ::mNeonGreen-15aa-ftsZ, amyE::erm-*$P_{hyperspank}$*-ftsA*] was created by transforming bAB185 with genomic DNA from bAB94.

**bAB209** [*ftsZ::mNeonGreen-15aa-ftsZ, amyE::*$P_{XylA}$*-mciZ (cat)*] was created by transforming bAB185 with genomic DNA from AH93.

**bAB213** [*ftsAZ::erm-ftsA-HaloTag(SW)-ftsZ-cat*] was created by inserting HaloTag between helices 6 and 7 of FtsA, the equivalent of a sandwich fusion (SW) that proved to be functional for MreB-mCherry (38). PY79 cells were transformed with a Gibson assembly consisting of 3 fragments: 1) PCR with primers oAB74 and oAB33 and template bAB163 genomic DNA (containing the region beginning upstream of the *ftsAZ* promoters and including the first 801 bp of the *ftsA* gene, *erm* cassette included); 2) PCR with primers oAB21 and oAB44 and the synthetic *HaloTag* gene as template (ordered from DNA 2.0, see fluorophore sequences section); 3) PCR with primers oAB48 and oAB30 and template bAB167 genomic DNA (containing the region from the last 522 bp of the *ftsA* gene to downstream of the *ftsAZ* terminators, *cat* cassette included). Proper integration was confirmed by PCR and sequencing.

**bAB215** [*amyE::erm-*$P_{hyperspank}$*-ftsAZ(D213A)*] was created by transforming PY79 with a Gibson assembly consisting of 3 fragments: 1) PCR with primers oMD191 and oMD232 and bMD352 genomic DNA template (containing the region upstream of the *amyE* gene, the *erm* cassette and the $P_{hyperspank}$ promoter); 2) PCR with primers oAB78 and oAB124 and bAB98 genomic DNA template (containing the first 2047 bp of the *ftsAZ* operon, inserting the

mutation GCT at bp 638 of the *ftsZ* gene); 3) PCR with primers oMD123 and oMD197 and bAB98 genomic DNA template (containing the last 529 bp of the *ftsZ* gene, inserting the mutation GCT at the 638 bp position of the *ftsZ* gene, and the region downstream of *amyE*).

**bAB217** [*amyE::erm-*$P_{hyperspank}$*-ftsA-mNeonGreen(SW)-ftsZ(D213A)*] was created by transforming PY79 with a Gibson assembly consisting of 3 fragments: 1) PCR with primers oMD191 and oMD232 and bMD352 genomic DNA template (containing the region upstream of the *amyE* gene, the *erm* cassette and the $P_{hyperspank}$ promoter); 2) PCR with primers oAB78 and oAB124 and bAB163 genomic DNA template (containing the first 2845 bp of the *ftsA-mNeonGreen( SW)-ftsZ* operon, inserting the mutation GCT at bp 638 of the *ftsZ* gene); 3) PCR with primers oAB123 and oMD197 and bAB98 genomic DNA template (containing the last 529 bp of the *ftsZ* gene, inserting the mutation GCT at the 638 bp position of the *ftsZ* gene, and the region downstream of *amyE*).

**bAB219** [*amyE::erm-*$P_{hyperspank}$*-ftsA-mNeonGreen-15aa-ftsZ*] was created by transforming PY79 with a Gibson assembly consisting of 3 fragments: 1) PCR with primers oMD191 and oMD232 and bMD352 genomic DNA template (containing the region upstream of the *amyE* gene, the *erm* cassette and the $P_{hyperspank}$ promoter); 2) PCR with primers oAB78 and oAB94 and bAB185 genomic DNA template (containing the *ftsA-mNeonGreen-15aa-ftsZ* operon); 3) PCR with primers oMD196 and oMD197 and PY79 genomic DNA template (containing the region downstream of *amyE*).

**bAB221** [*ftsZ::mNeonGreen-15aa-ftsZ, amyE::erm-*$P_{hyperspank}$*-ftsA-mNeonGreen-15aa-ftsZ*] was created by transforming bAB185 with genomic DNA from bAB219.

**bAB229** [*ftsAZ::erm-ftsA-HaloTag(SW)-mNeonGreen-15aa-ftsZ-cat*] was created by transforming PY79 with a Gibson assembly consisting of 2 fragments: 1) PCR with primers oAB74 and oAB44 and template bAB213 genomic DNA (containing the region from upstream of the *ftsAZ* promoters to the end of the *HaloTag* gene, *erm* cassette included); 2) PCR with primers oAB48 and oAB30 and template bAB181 genomic DNA (containing the region from the last 522 bp of the *ftsA* gene to downstream of the *ftsAZ* terminators, *cat* cassette included). Proper integration was confirmed by PCR and sequencing.

**bAB248** [*ftsZ::mNeonGreen-15aa-ftsZ, amyE::*$P_{hyperspank}$*-minCD (spc)*] was created by transforming bAB185 with genomic DNA from JB60 (a gift from Frederico Gueiros Filho).

**bAB270** [*pbp2B::mNeonGreen-15aa-pbp2B, ftsZΩftsZ(T111A) (tet)*] was created by transforming ME7 with genomic DNA from AB62 (a gift from Frederico Gueiros Filho).

**bAB271** [*pbp2B::mNeonGreen-15aa-pbp2B, ftsZΩftsZ(G106S) (tet)*] was created by transforming ME7 with genomic DNA from Z-84 (a gift from Frederico Gueiros Filho).

**bAB272** [*pbp2B::mNeonGreen-15aa-pbp2B, amyE::erm-*$P_{hyperspank}$*-ftsAZ*] was created by transforming ME7 with genomic DNA from bAB98.

**bAB273** [*pbp2B::mNeonGreen-15aa-pbp2B, amyE::erm-*$P_{hyperspank}$*-ftsAZ(D213A)*] was created by transforming ME7 with genomic DNA from bAB215.

**bAB274** [*pbp2B::mNeonGreen-15aa-pbp2B, amyE::$P_{XylA}$-mciZ (cat)*] was created by transforming ME7 with genomic DNA from AH93.

**bAB281** [*amyE::erm-$P_{hyperspank}$-ftsA-mNeonGreen-15aa-ftsZ, ftsZΩftsZ(T111A) (tet)*] was created by transforming bAB219 with genomic DNA from AB62 (a gift from Frederico Gueiros Filho).

**bAB282** [*amyE::erm-$P_{hyperspank}$-ftsA-mNeonGreen-15aa-ftsZ, ftsZΩftsZ(G106S) (tet)*] was created by transforming bAB219 with genomic DNA from Z-G106S (a gift from Frederico Gueiros Filho).

**bAB285** [*pbp2B::mNeonGreen-15aa-pbp2B, amyE::$P_{hyperspank}$-minCD (spc)*] was created by transforming ME7 with genomic DNA from JB60 (a gift from Frederico Gueiros Filho).

**bAB310** [*pbp2B::mNeonGreen-15aa-pbp2B, amyE::erm-$P_{hyperspank}$-ftsA*] was created by transforming ME7 with genomic DNA from bAB94.

**SH013** [*trpC2, ftsZ:: ftsZ-GFP::cat*] was created by transforming *B. subtilis* 168CA [*trpC2*] with genomic DNA from PL642 (a gift from Petra Anne Levin).

**SH033** [*trpC2, ftsZ:: ftsZ-GFP::cat, Δhag::aph(Kan)*] was created by transforming SH013 with genomic DNA from PB5250 (obtained from BGSC catalogue number 1A842).

**SH41** [*ftsZ::mNeonGreen-15aa-ftsZ, Δhag::aph (Kan*)] was created by transforming bAB185 with genomic DNA from PB5250 (obtained from BGSC catalogue number 1A842).

## Supplementary Material

Refer to Web version on PubMed Central for supplementary material.

## Acknowledgments

We thank F. Gueiros-Filho, R. Losick, M. Erb, and P. Levin for strains; J Xiao for discussions; L. Lavis for JF dyes; B. Murphy and E. Pasciak for FDAA synthesis help; F. Gueiros-Filho, R. Daniel and J. Errington for antibodies; R. Losick, B. LaSarre, and D. Kearns for comments. This work was supported by NIH grants GM113172 to MSV and YVB; GM51986 to YVB; DP2AI117923-01 to ECG; a Newcastle University Research Fellowship and Royal Society Research Grant RG150475 to SH; a Science Without Borders Research Fellowship to AWB-F; an ERC Advanced Grant SynDiv 669598 to CD, and an NSF GRFP (DGE1144152) to GRS. SIM was performed in the Indiana University Light Microscopy Imaging Center supported by S10RR028697-01

## References

1. Chen Y, Erickson HP. Rapid in vitro assembly dynamics and subunit turnover of FtsZ demonstrated by fluorescence resonance energy transfer. J Biol Chem. 2005; 280:22549–22554. [PubMed: 15826938]
2. Szwedziak P, Wang Q, Bharat TAM, Tsim M, Lowe J. Architecture of the ring formed by the tubulin homologue FtsZ in bacterial cell division. Elife. 2014; 3:e04601. [PubMed: 25490152]
3. Ma X, Ehrhardt DW, Margolin W. Colocalization of cell division proteins FtsZ and FtsA to cytoskeletal structures in living Escherichia coli cells by using green fluorescent protein. Proc Natl Acad Sci USA. 1996; 93:12998–13003. [PubMed: 8917533]
4. Gamba P, Veening JW, Saunders NJ, Hamoen LW, Daniel RA. Two-step assembly dynamics of the Bacillus subtilis divisome. J Bacteriol. 2009; 191:4186–4194. [PubMed: 19429628]

5. Kuru E, et al. In Situ probing of newly synthesized peptidoglycan in live bacteria with fluorescent D-amino acids. Angew Chem Int Ed Engl. 2012; 51:12519–12523. [PubMed: 23055266]
6. Lupoli TJ, et al. Transpeptidase-Mediated Incorporation of d-Amino Acids into Bacterial Peptidoglycan. J Am Chem Soc. 2011; 133:10748–10751. [PubMed: 21682301]
7. Eberhardt C, Kuerschner L, Weiss DS. Probing the catalytic activity of a cell division-specific transpeptidase in vivo with beta-lactams. J Bacteriol. 2003; 185:3726–3734. [PubMed: 12813065]
8. Thanedar S, Margolin W. FtsZ Exhibits Rapid Movement and Oscillation Waves in Helix-like Patterns in Escherichia coli. Current Biology. 2004; 14:1167–1173. [PubMed: 15242613]
9. Rowlett VW, Margolin W. 3D-SIM super-resolution of FtsZ and its membrane tethers in Escherichia coli cells. Biophys J. 2014; 107:L17–20. [PubMed: 25418183]
10. Coltharp C, Buss J, Plumer TM, Xiao J. Defining the rate-limiting processes of bacterial cytokinesis. Proc Natl Acad Sci USA. 2016; 113:E1044–E1053. [PubMed: 26831086]
11. Holden SJ, et al. High throughput 3D super-resolution microscopy reveals Caulobacter crescentus in vivo Z-ring organization. Proc Natl Acad Sci USA. 2014; 111:4566–4571. [PubMed: 24616530]
12. Strauss MP, et al. 3D-SIM Super Resolution Microscopy Reveals a Bead-Like Arrangement for FtsZ and the Division Machinery: Implications for Triggering Cytokinesis. PLoS Biol. 2012; 10doi: 10.1371/journal.pbio.1001389
13. Anderson DE, Gueiros-Filho FJ, Erickson HP. Assembly dynamics of FtsZ rings in Bacillus subtilis and Escherichia coli and effects of FtsZ-regulating proteins. J Bacteriol. 2004; 186:5775–5781. [PubMed: 15317782]
14. Grimm JB, et al. A general method to improve fluorophores for live-cell and single-molecule microscopy. Nat Meth. 2015; 12:244–250.
15. Garner EC, et al. Coupled, circumferential motions of the cell wall synthesis machinery and MreB filaments in B. subtilis. Science. 2011; 333:222–225. [PubMed: 21636745]
16. Loose M, Mitchison TJ. The bacterial cell division proteins FtsA and FtsZ self-organize into dynamic cytoskeletal patterns. Nat Cell Biol. 2014; 16:38–46. [PubMed: 24316672]
17. Niu L, Yu J. Investigating intracellular dynamics of FtsZ cytoskeleton with photoactivation single-molecule tracking. Biophys J. 2008; 95:2009–2016. [PubMed: 18390602]
18. Redick SD, Stricker J, Briscoe G, Erickson HP. Mutants of FtsZ targeting the protofilament interface: effects on cell division and GTPase activity. J Bacteriol. 2005; 187:2727–2736. [PubMed: 15805519]
19. Haydon DJ, et al. An Inhibitor of FtsZ with Potent and Selective Anti-Staphylococcal Activity. Science. 2008; 321:1673–1675. [PubMed: 18801997]
20. Bisson-Filho AW, et al. FtsZ filament capping by MciZ, a developmental regulator of bacterial division. Proc Natl Acad Sci USA. 2015; 112:E2130–E2138. [PubMed: 25848052]
21. Yang X, et al. GTPase activity-coupled treadmilling of the bacterial tubulin FtsZ organizes septal cell-wall synthesis. 2016:077610. bioRxiv.
22. Osawa M, Erickson HP. Liposome division by a simple bacterial division machinery. Proc Natl Acad Sci USA. 2013; 110:11000–11004. [PubMed: 23776220]
23. Egan AJF, Vollmer W. The stoichiometric divisome: a hypothesis. Front Microbiol. 2015; 6:0–6.
24. Li Z, Trimble MJ, Brun YV, Jensen GJ. The structure of FtsZ filaments in vivo suggests a force-generating role in cell division. EMBO J. 2007; 26:4694–4708. [PubMed: 17948052]
25. Kuru E, Tekkam S, Hall E, Brun YV, Van Nieuwenhze MS. Synthesis of fluorescent D-amino acids and their use for probing peptidoglycan synthesis and bacterial growth in situ. Nature protocols. 2015; 10:33–52. [PubMed: 25474031]
26. Wang HC, Gayda RC. High-level expression of the FtsA protein inhibits cell septation in Escherichia coli K-12. Journal of bacteriology. 1990; 172:4736–4740. [PubMed: 2198274]
27. Dewar SJ, Begg KJ, Donachie WD. Inhibition of cell division initiation by an imbalance in the ratio of FtsA to FtsZ. J Bacteriol. 1992; 174:6314–6316. [PubMed: 1400183]
28. Araujo-Bazan L, Ruiz-Avila LB, Andreu D, Huecas S, Andreu JM. Cytological Profile of Antibacterial FtsZ Inhibitors and Synthetic Peptide MciZ. Frontiers in microbiology. 2016; 7:1558. [PubMed: 27752253]

29. Handler AA, Lim JE, Losick R. Peptide inhibitor of cytokinesis during sporulation in Bacillus subtilis. Mol Microbiol. 2008; 68:588–599. [PubMed: 18284588]
30. Nick Perry J-YT, Schindelin Johannes. TrackMate. 2012
31. Wu F, van Schie BGC, Keymer JE, Dekker C. Symmetry and scale orient Min protein patterns in shaped bacterial sculptures. Nature nanotechnology. 2015; 10:719–726.
32. Mannik J, et al. Robustness and accuracy of cell division in Escherichia coli in diverse cell shapes. Proceedings of the National Academy of Sciences of the United States of America. 2012; 109:6957–6962. [PubMed: 22509007]
33. de Jong IG, Beilharz K, Kuipers OP, Veening J-W. Live Cell Imaging of Bacillus subtilis and Streptococcus pneumoniae using Automated Time-lapse Microscopy. Journal of visualized experiments : JoVE. 2011
34. Schindelin J, et al. Fiji: an open source platform for biological image analysis. Nature Methods. 2012; 9:676–682. [PubMed: 22743772]
35. Ball G, et al. SIMcheck: a Toolbox for Successful Super-resolution Structured Illumination Microscopy. Scientific reports. 2015; 5:15915. [PubMed: 26525406]
36. Hoffman H. Simple violin plot using matlab default kernel density estimation. 2015
37. Zoergiebel F. PLOTERR general error bar plot. 2008
38. Bendezu FO, Hale CA, Bernhardt TG, de Boer PAJ. RodZ (YfgA) is required for proper assembly of the MreB actin cytoskeleton and cell shape in E. coli. The EMBO journal. 2009; 28:193–204. [PubMed: 19078962]
39. Lee TK, Meng K, Shi H, Huang KC. Single-molecule imaging reveals modulation of cell wall synthesis dynamics in live bacterial cells. Nature communications. 2016; 7:13170.
40. Cho H, et al. Bacterial cell wall biogenesis is mediated by SEDS and PBP polymerase families functioning semi-autonomously. Nature microbiology. 2016:16172.
41. Youngman PJ, Perkins JB, Losick R. Genetic transposition and insertional mutagenesis in Bacillus subtilis with Streptococcus faecalis transposon Tn917. Proc Natl Acad Sci U S A. 1983; 80:2305–2309. [PubMed: 6300908]
42. Blasios V, et al. Genetic and Biochemical Characterization of the MinC-FtsZ Interaction in Bacillus subtilis. PLoS ONE. 2013; 8
43. Kunst F, et al. The complete genome sequence of the gram-positive bacterium Bacillus subtilis. Nature. 1997; 390:249–256. [PubMed: 9384377]
44. Levin PA, Kurtser IG, Grossman AD. Identification and characterization of a negative regulator of FtsZ ring formation in Bacillus subtilis. Proc Natl Acad Sci U S A. 1999; 96:9642–9647. [PubMed: 10449747]
45. Senesi S, et al. Surface-associated flagellum formation and swarming differentiation in Bacillus subtilis are controlled by the ifm locus. Journal of bacteriology. 2004; 186:1158–1164. [PubMed: 14762011]

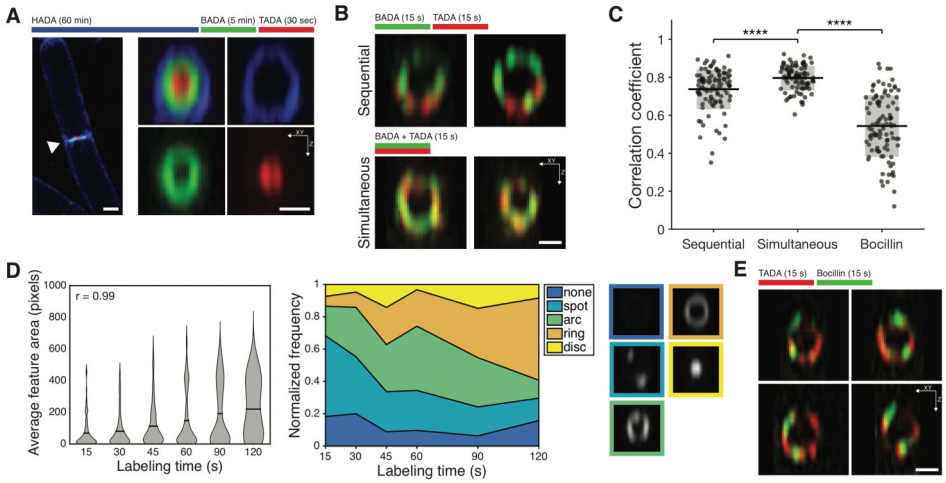


**Figure 1. Septal PG synthesis occurs at discrete, mobile sites**

**A** Sequential FDAA labeling of division septa shows outside-in synthesis. (Right) 90° rotations of septa.

**B** Sites of PG synthesis move around the septum.

**C** Correlation coefficient of overlap between colors in B and E. Line: mean, box: SD.

**D** FDAA labeling proceeds from puncta to complete rings. (Left) Area of FDAA features increases with pulse length. Lines: mean, r: correlation coefficient of the means. (Center) Blinded classification of FDAA features at various pulse lengths. (Right) representative images of septal PG structures.

**E** Sites of PG synthesis are offset from synthetic enzymes. Colored bars indicate time course of FDAA labeling. All images taken with 3D-SIM. Scale bars: 0.5 μm.

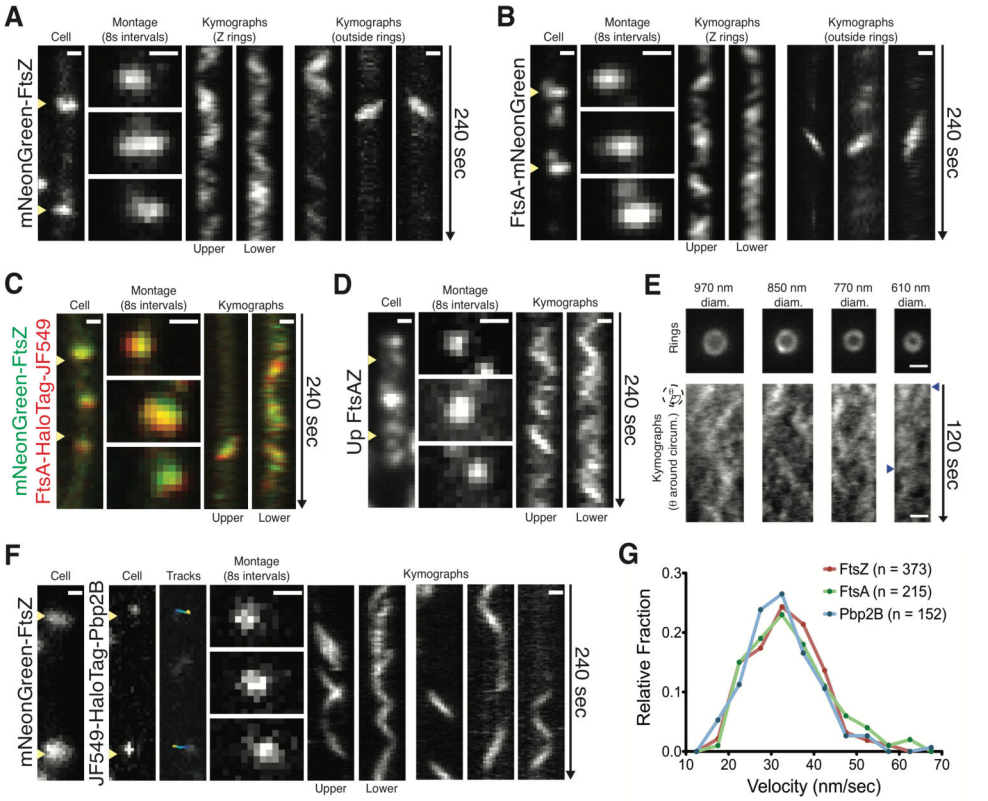


**Figure 2. FtsAZ and Pbp2B move directionally around the division site**

**A** mNeonGreen-FtsZ (bAB185) shows directional motion inside (left) and outside (right) the Z ring.

**B** FtsA-mNeonGreen (bAB167) shows directional motion inside (left) and outside (right) the ring.

**C** mNeonGreen-FtsZ and FtsA-HaloTag-JF549 (bAB229) colocalize and move together.

**D** FtsAZ overexpression (100 μM IPTG in bAB221) creates increased FtsZ filaments showing directional motion outside the Z ring.

**E** Vertically immobilized cells (SH41) show multiple, independent mNeonGreen-FtsZ filaments moving in both directions around the division site. Cropped rings and radial kymographs in early (left), mid (center), and late (right) divisional stages. Blue arrows indicate directional FtsZ tracks.

**F** Single molecules of Pbp2B (bGS31, 15 min incubation of 50 pM JF549) move directionally around the division site. Blue to yellow indicates trajectory time.

**G** Velocity distributions of FtsA filaments, FtsZ filaments, and single Pbp2B molecules. Kymographs drawn at yellow arrows. Scale bars = 0.5 μm

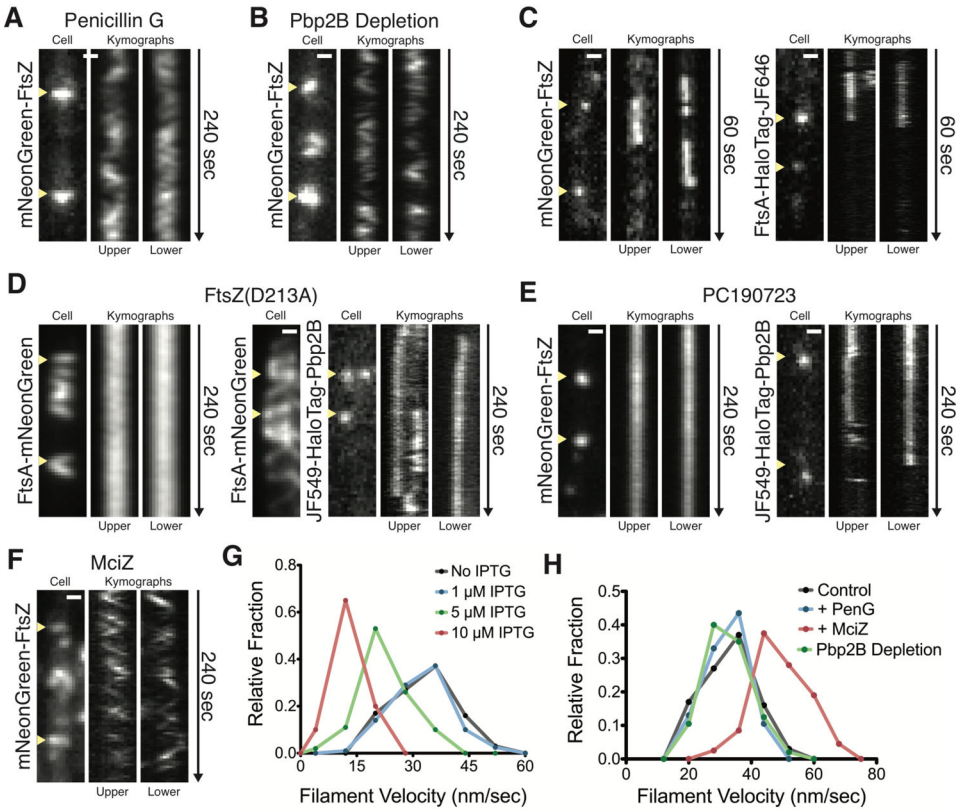


**Figure 3. Directional FtsAZ motion is driven by treadmilling, independent of cell wall synthesis, and required for Pbp2B motion**

**A** FtsZ continues to move directionally after treatment with Penicillin G. bAB185 imaged 5 minutes after addition of 3 μl of 10 mg/ml penicillin G to an agarose pad.

**B** FtsZ continues to move directionally after Pbp2B depletion. Before imaging, bGS31 was grown without IPTG until no divisions were observed (3 hours).

**C** Single molecules of FtsZ and FtsA are immobile within the division site. Single molecules were obtained by growing bAB219 with no IPTG (left) or bAB229 with 15 min of 250 pM JF646 (right).

**D** Overexpression of GTPase-deficient FtsZ stops FtsZ and Pbp2B motion. bAB217 (left) and bGS90 (right) were imaged after induction of FtsZ(D213A) (100 μM IPTG, 1 hour).

**E** Directional motion of FtsZ and Pbp2B is stopped by PC190723. bAB185 (left) and bGS31 with 15 min incubation of 50 pM JF549 (right) 5 minutes after addition of 10 μM PC190723.

**F** FtsZ velocity increases following exposure to MciZ. bAB185 was imaged following addition of 1 μM MciZ in a microfluidic device.

**G** Velocity distributions of FtsZ filaments (bAB217) at different levels of FtsZ(D213A) induction.

**H** Velocity distributions of FtsZ filaments under different perturbations.

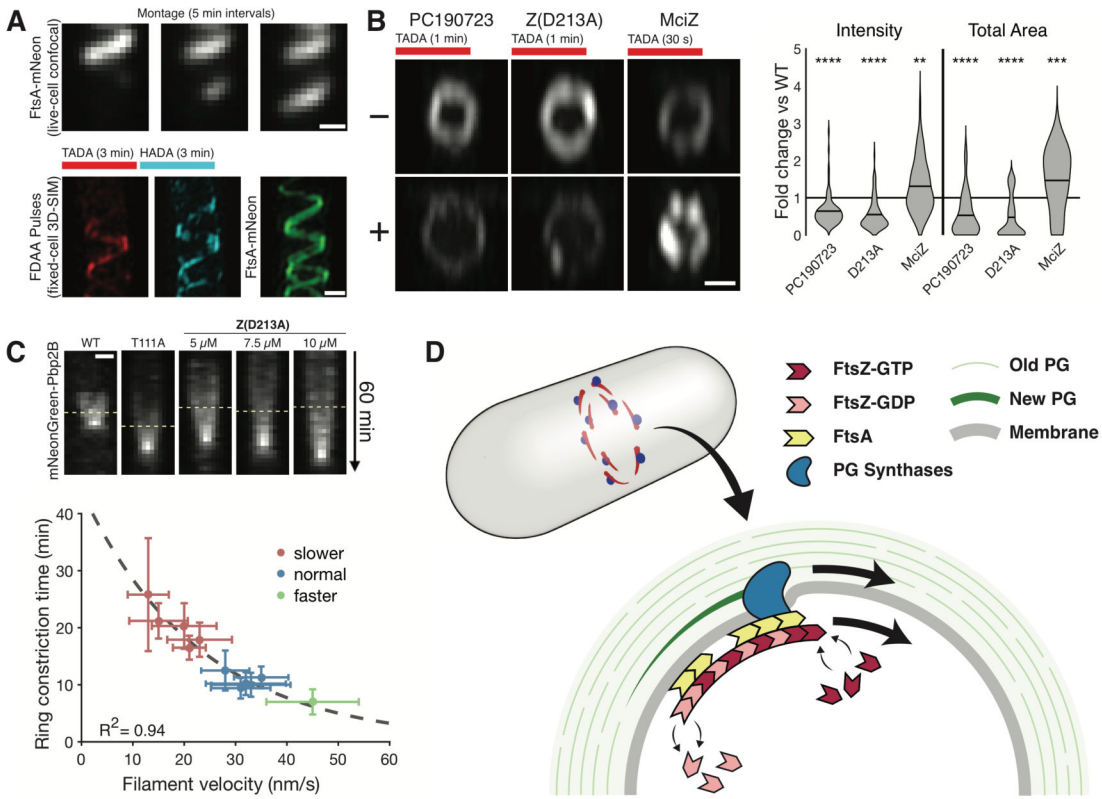


**Figure 4. Cytokinesis is controlled by directional motion of FtsAZ filaments**

**A** FtsZ(D213A) overexpression (1 mM IPTG in bAB217) produces slowly growing FtsA spirals with spiral FDAA insertion. (Top) Montage of growing FtsA spiral acquired with spinning-disk confocal. (Bottom) Sequential FDAA labeling and FtsA localization imaged with 3DSIM in a fixed cell.

**B** Altering FtsZ velocity changes the amount and total area of FDAA incorporation. (left) PY79 with 1 μg/ml PC190723, 10 min, (middle) bAB217 with 20 μM IPTG for 1 hour, (right) AH93 with 50 mM xylose, 5 min. Following treatment, cells were incubated with TADA for time indicated, fixed, then imaged with 3D-SIM. (Far right) Total intensity and area of septal FDAA incorporation. Lines: mean.

**C** Cytokinesis scales with FtsZ treadmilling velocity. For each condition, pairs of strains were used to measure 1) FtsZ velocity (using mNeonGreen-FtsZ) and 2) septation rates (using mNeonGreen-Pbp2B). (Top) Kymographs of constricting Pbp2B rings in different FtsZ backgrounds (line marks start of constriction). (Bottom) Plot of constriction time vs. FtsZ velocity in different conditions. Treadmilling velocity and septation rates were acquired in identical conditions, save for measurements with MciZ (see SOM). Error bars: SD of the mean.

**D** Model for treadmilling-coupled cell division. (Top) The Z ring contains multiple FtsAZ filaments that treadmill around the division plane, pulling associated PG synthases. (Bottom) FtsZ treadmilling both regulates and distributes the activity of the PG synthases, building sequentially smaller uniform arcs of PG to divide the cell.